

APPLICABILITY OF FLOW SIMULATION MODELS TO THE CASE OF RADIAL INFLOW ONTO A ROTATING CORE

RAFAŁ BIERNACKI

*Mechanical Engineering Department,
Technical University of Gdansk,
Narutowicza 11/12, 80-952 Gdansk, Poland
rbiernac@pg.gda.pl*

(Received 10 January 2001; revised manuscript received 22 January 2001)

Abstract: The paper presents the results of fluid flow simulations carried out by means of the FIDAP7.6 program (a fluid dynamics FEM package) for the case of radial inflow onto a rotating shaft. The particular geometric configuration has been chosen to resemble a generalized inlet chamber of twin low-pressure steam turbines, but with the axial outlet section extended to allow better observation of flow instabilities in that region.

The calculations were carried out for the same channel geometry for both compressible and incompressible flow, using the same or slightly varying boundary conditions. Extensive variation in non-physical parameters of the model was explored, such as applying different meshes over the region, as well as utilizing different turbulence and upwinding models.

The intent of this research was to evaluate the relative applicability of the various available flow models to the simulation of axisymmetric flows with steep velocity gradients, and to discover the limitations of these models. The calculations have in fact established significant differences in the behavior of the simulated flow for the different meshes and models. Some results were characterized by extensive areas of recirculating flow whereas others, for the same boundary conditions, showed no recirculation. Correct near-wall meshing as well as the choice of the upwinding scheme were established as the critical factors in this regard. There was also noticeable variation in outlet velocity profiles.

An extensive zone of separation within the investigated channel as well as a standing annular vortex near the point of stagnation are flow features of some interest. These patterns of flow change in response to the changing non-physical parameters; the separation zone in particular is absent or slow to develop under some setups.

The influence of inflow parameters, the initial velocity distribution and turbulent intensity in particular, on flow behavior in contact with the rotating shaft have also been an area of investigation, as these are often defined with considerable uncertainty in practical applications. It was observed that some latitude in assuming these parameters did not significantly alter the relevant flow parameters at outlet (the velocity and pressure distributions), although it did induce variation in other aspects of the flow (such as the extent of the standing vortex).

Keywords: turbulent flow, numerical flow simulation, steam turbine, turbine inlet, flow structures

1. Introduction

The particular geometric configuration has been chosen to resemble a generalized inlet chamber of twin low-pressure steam turbines [1]. It contains flow features intrinsic to these inlets, such as fixed and rotating walls, transition of radial into axial flow, corners and localized regions of acceleration. Prior to this work considerable investigation has been made into similar flow configuration in an actual turbine inlet [2], but proprietary issues prevent its publication. In order to generalize the results and investigate flow behavior independently of minor configuration details, the geometry has here been simplified in comparison to an actual inlet chamber. The flow is axisymmetric, with a radial inflow region and a bidirectional axial outlet. The axial outlet section has been extended to allow better observation of flow instabilities in that region.

2. Modeled flow configuration

Figure 1 shows the configuration and dimensions of the investigated flow. The region consists of two cylinders coaxial with a central rotating shaft. Fluid enters the region radially through the perimeter of the outer cylinder and leaves through the bases of the inner cylinder. Inflow velocity is 25 m/s.

For all the variants the same boundary conditions were assigned, as specified in Figure 2. For the inlet surface the turbulence parameters k and ϵ were estimated based on the assumed turbulent intensity at inlet, using the approximate formulas:

$$\text{turbulent kinetic energy} \quad k = 1.5(I \times u_\infty)^2 \quad (1)$$

$$\text{dissipation} \quad \epsilon = \frac{k^{1.5}}{0.1\delta} \quad (2)$$

where δ is the characteristic dimension of the inlet, and turbulent intensity I for the simulated flow varies between 0 and 0.10. A variant was also modeled for which the inflow velocity was zero, and fluid motion was induced by shaft rotation only.

3. Turbulence models

The majority of turbulence models used in practice are two-equation models, in which the system of equations describing fluid motion is augmented by introducing two additional variables, typically the turbulent kinetic energy k and dissipation ϵ [3]. In the most common k - ϵ model, the system of equations is then closed with the equations:

$$\rho \left(\frac{\partial k}{\partial t} + u_j \frac{\partial k}{\partial x_j} \right) = \frac{\partial}{\partial x_j} \left[\left(\mu + \frac{\mu_t}{\sigma_k} \right) \frac{\partial k}{\partial x_j} \right] + \mu_t \left(\frac{\partial u_i}{\partial x_j} + \frac{\partial u_j}{\partial x_i} \right) \frac{\partial u_i}{\partial x_j} - \rho \epsilon \quad (3)$$

$$\rho \left(\frac{\partial \epsilon}{\partial t} + u_j \frac{\partial \epsilon}{\partial x_j} \right) = \frac{\partial}{\partial x_j} \left[\left(\mu + \frac{\mu_t}{\sigma_\epsilon} \right) \frac{\partial \epsilon}{\partial x_j} \right] + c_1 \frac{\epsilon}{k} \mu_t \left(\frac{\partial u_i}{\partial x_j} + \frac{\partial u_j}{\partial x_i} \right) \frac{\partial u_i}{\partial x_j} - c_2 \rho \frac{\epsilon^2}{k} \quad (4)$$

where the eddy viscosity $\mu_t = \rho c_\mu \frac{k^2}{\epsilon}$, and the constants are assigned the following values: $c_\mu = 0.09$, $\sigma_k = 1.00$, $\sigma_\epsilon = 1.30$, $c_1 = 1.44$, $c_2 = 1.92$.

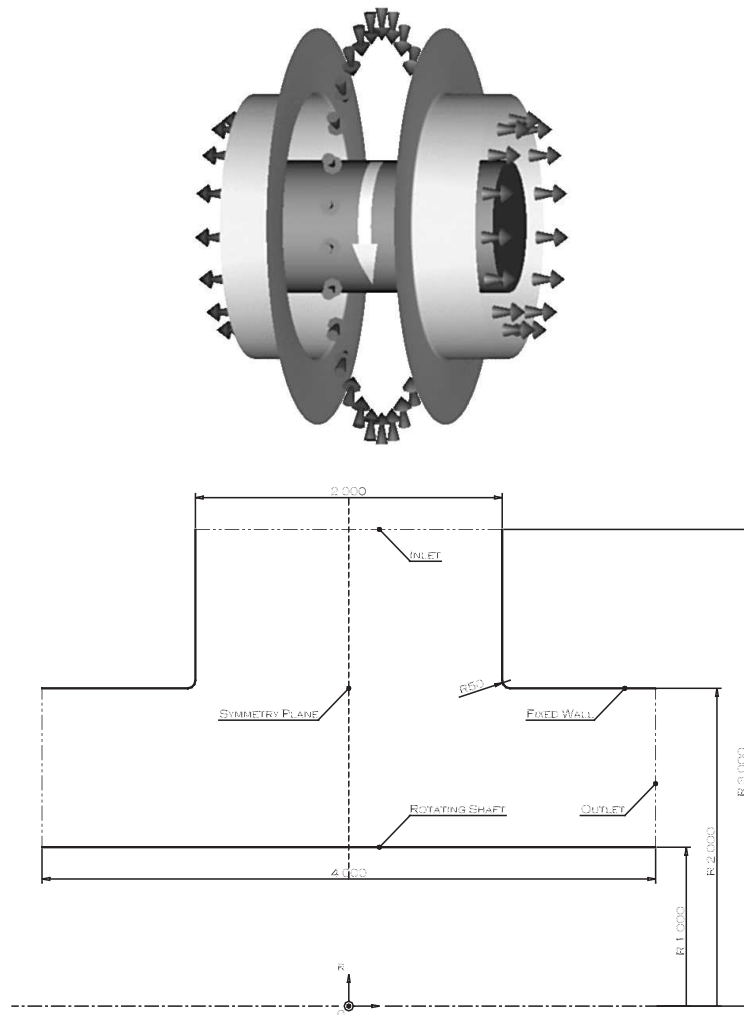


Figure 1. Shape and dimensions of the investigated inlet

In the extended $k-\varepsilon$ model, with the introduction of an additional constant c_4 , Equation (4) takes the form:

$$\rho \left(\frac{\partial \varepsilon}{\partial t} + u_j \frac{\partial \varepsilon}{\partial x_j} \right) = \frac{\partial}{\partial x_j} \left[\left(\mu_0 + \frac{\mu_t}{\sigma_\varepsilon} \right) \frac{\partial \varepsilon}{\partial x_j} \right] + c_1 \frac{\varepsilon}{k} \mu_t \left(\frac{\partial u_i}{\partial x_j} + \frac{\partial u_j}{\partial x_i} \right) \frac{\partial u_i}{\partial x_j} + c_4 \frac{1}{\rho k} \left[\mu_t \left(\frac{\partial u_i}{\partial x_j} + \frac{\partial u_j}{\partial x_i} \right) \frac{\partial u_i}{\partial x_j} \right]^2 - c_2 \rho \frac{\varepsilon^2}{k} \quad (4a)$$

and the existing constants are assigned the variant values: $c_\mu = 0.09$, $\sigma_k = 0.75$, $\sigma_\varepsilon = 1.15$, $c_1 = 1.15$, $c_2 = 1.9$, $c_4 = 0.25$.

In the RNG model the Equations (3) and (4) have the form:

$$\rho \left(\frac{\partial k}{\partial t} + u_j \frac{\partial k}{\partial x_j} \right) = \frac{\partial}{\partial x_j} \left[\left(\mu + \frac{\mu_t}{\sigma_k} \right) \frac{\partial k}{\partial x_j} \right] + \mu_t \left(\frac{\partial u_i}{\partial x_j} + \frac{\partial u_j}{\partial x_i} \right) \frac{\partial u_i}{\partial x_j} - \rho \varepsilon \quad (3b)$$

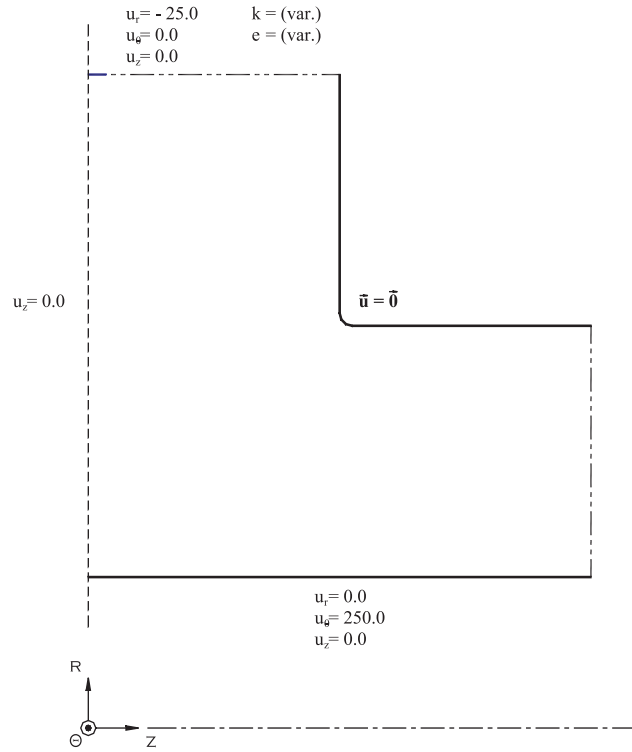


Figure 2. Boundary conditions

$$\rho \left(\frac{\partial \varepsilon}{\partial t} + u_j \frac{\partial \varepsilon}{\partial x_j} \right) = \frac{\partial}{\partial x_j} \left[\left(\mu + \frac{\mu_t}{\sigma_\varepsilon} \right) \frac{\partial \varepsilon}{\partial x_j} \right] + c_1 \frac{\varepsilon}{k} \mu_t \left(\frac{\partial u_i}{\partial x_j} + \frac{\partial u_j}{\partial x_i} \right) \frac{\partial u_i}{\partial x_j} - \frac{c_\mu \eta^3 (1 - \eta / \eta_0) \varepsilon^2}{1 + \beta \eta^3} \frac{\varepsilon^2}{k} - c_2 \rho \frac{\varepsilon^2}{k} \quad (4b)$$

where $\eta = \frac{k}{\varepsilon} \sqrt{\left(\frac{\partial u_i}{\partial x_j} + \frac{\partial u_j}{\partial x_i} \right) \frac{\partial u_i}{\partial x_j}}$, and the constants are: $c_\mu = 0.085$, $\sigma_k = 0.7179$, $\sigma_\varepsilon = 0.7179$, $c_1 = 1.42$, $c_2 = 1.68$, $\eta_0 = 4.38$, $\beta = 0.015$.

An “improved” RNG model is also employed, with the constants: $c_\mu = 0.0865$, $\sigma_k = 0.7179$, $\sigma_\varepsilon = 0.7179$, $c_1 = 1.45$, $c_2 = 1.83$, $\eta_0 = 4.618$, $\beta = 0.017$.

There is also a turbulent frequency model, similar to the k - ε models above, but applicable mainly to low Reynolds number turbulent flow simulations. This model is not appropriate for the flow considered here.

4. Influence of computational mesh

The crucial criterion for the applicability of a given computational mesh to the simulation of a particular flow is supplied by the nondimensional wall distance y^+ , described by the formula:

$$y^+ = \frac{\delta \sqrt{\rho \tau_w}}{\mu} \quad (5)$$

where δ is the normal wall distance and τ_w is shear stress at wall.

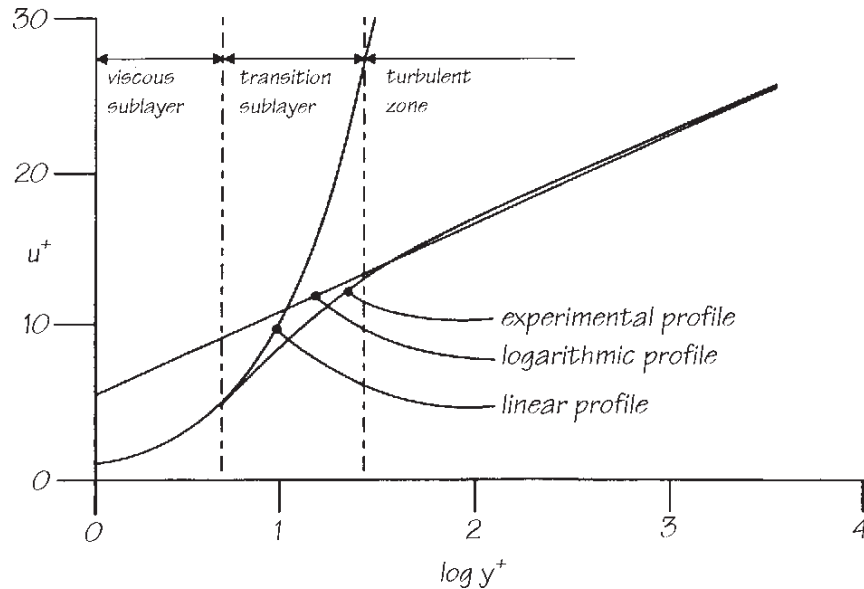


Figure 3. Nondimensional velocity profile within the boundary layer

The value of y^+ at a point in the flow indicates whether the point is contained within the viscous sublayer of the boundary layer, the transition sublayer, or the turbulent region (Figure 3).

The turbulence models listed above are not suitable for modeling flow within the boundary layer, where the flow is not fully turbulent. In flow simulation software, special wall functions are used for modeling flow in the viscous and transition sublayers. As, however, these wall functions are employed only within the single layer of mesh elements immediately adjacent to the wall, it follows that mesh pitch in the vicinity of the wall must be adjusted to ensure that the value of y^+ is kept within proper limits (> 30)¹ at the interface between the first and second layer of mesh elements. On the other hand, the mesh spacing should not be too coarse, as this may cause a reduced interaction between the wall and the flow. This aspect of mesh calibration was subject to particular scrutiny within this investigation. As it turned out, in some of the researched variants the use of a mesh that was too coarse has resulted in an inhibition of the boundary layer separation process (*cf.* Figure 5).

The value of y^+ at points within the flow, being a function of the flow, is not known beforehand but can only be ascertained after running the simulation. Thus the originally designed mesh often proves inadequate and must be readjusted after obtaining y^+ distribution from the first run. Figure 4 shows two such consecutive meshings for the problem under investigation.

1. For the $k-w$ model, which is optimized for modeling weakly turbulent flows, the value should be between $1 < y^+ < 30$.

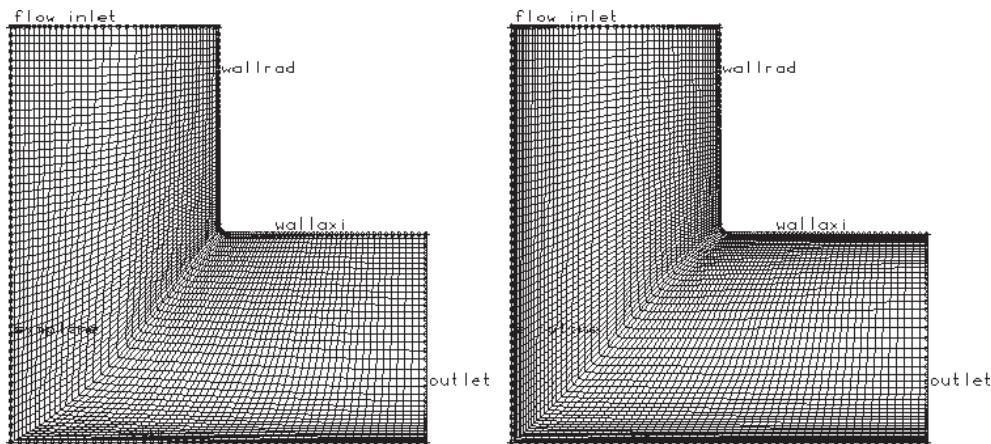


Figure 4. Consecutive approximations toward optimum mesh distribution at wall

5. Flow patterns

An extensive zone of separation (1 in Figure 5) within the investigated channel as well as a standing annular vortex 2 near the point of stagnation (actually twin vortices – one appears in each half of the symmetric flow region) are flow features of some interest.

These patterns of flow change in response to the changing non-physical parameters; the separation zone in particular is absent or slow to develop under some setups. As a separation may be expected to appear in a similarly configured actual turbine inlet duct², its appearance or absence in a simulated setup is a useful indication of the applicability of a given flow model.

The vortices 2 have the net effect of transporting the angular velocity of the shaft away from the shear zone at the shaft into the middle of the flow. This is not an undesirable feature, inasmuch as the fluid is thus angularly accelerated in a more gradual manner, reducing losses (energy dissipation in the flow is most marked within the shear zone). Temperature distribution is affected in a similar way (Figure 7). (In an actual turbine, the angular momentum which the shaft imparts to the fluid is itself caused by fluid interaction with rotor blades downstream from the investigated zone; it is, in a way, recirculating in the fluid-shaft system.)

Shaft motion introduces some turbulence into the flow; but the presence of an undesirable separation zone at B has a more pronounced effect in that regard, as may be observed in the vorticity plot, Figure 8.

The influence of inflow parameters, the initial velocity distribution and turbulent intensity in particular, on flow behavior in contact with the rotating shaft has also been an area of investigation, as these are often defined with considerable uncertainty in practical applications. As regards velocity distribution in the inlet area, two limiting cases were modeled: one with uniform velocity of 25 m/s across the inlet surface, and one with a parabolic velocity profile and the same overall flow rate as the uniform case. The actual velocity distribution in a turbine inlet must fall between these extremes, but may be expected

2. The sharp corner induces the zone of separation; it may be alleviated by rounding the corner, but more effectively by breaking the 90-degree bend into smaller, well-separated bends.

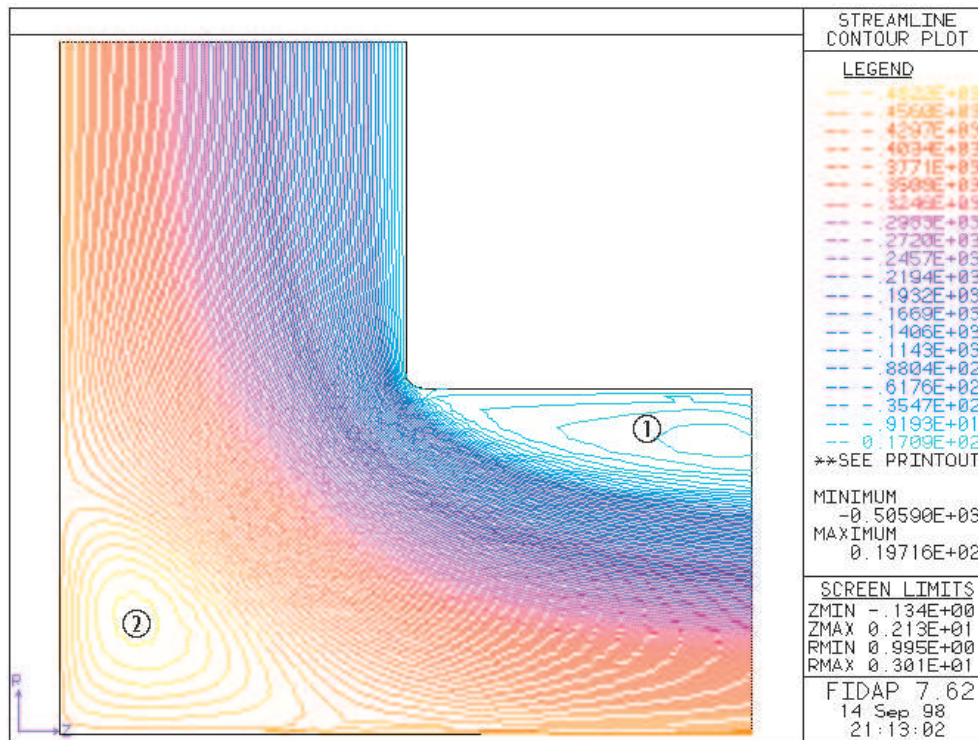


Figure 5. Streamline plot, compressible flow

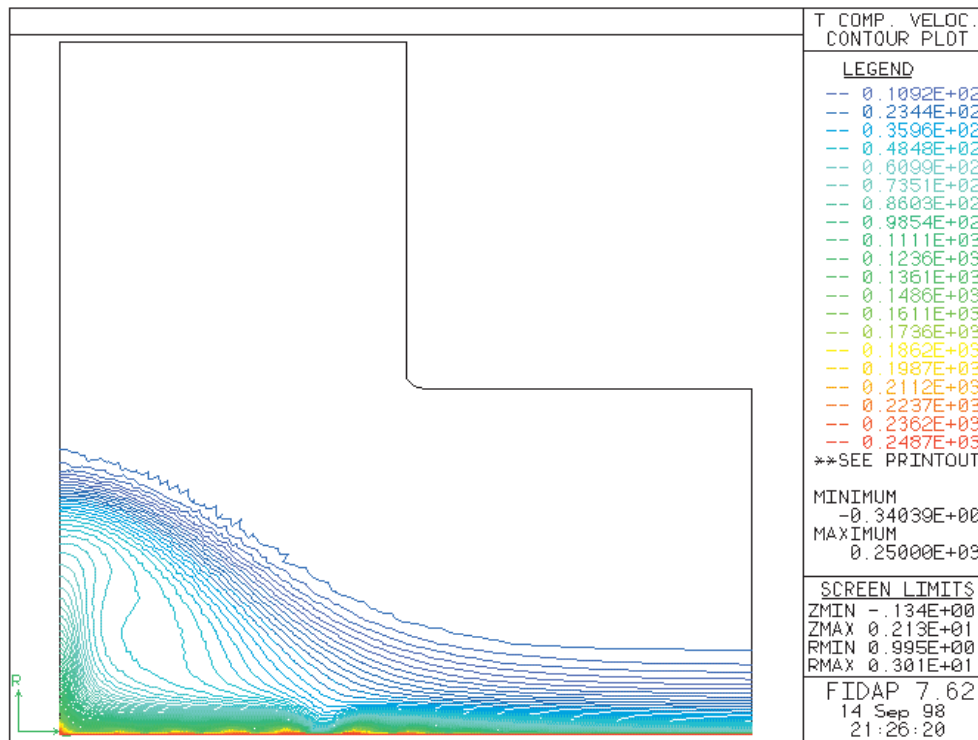


Figure 6. Angular velocity u_θ induced by shaft rotation

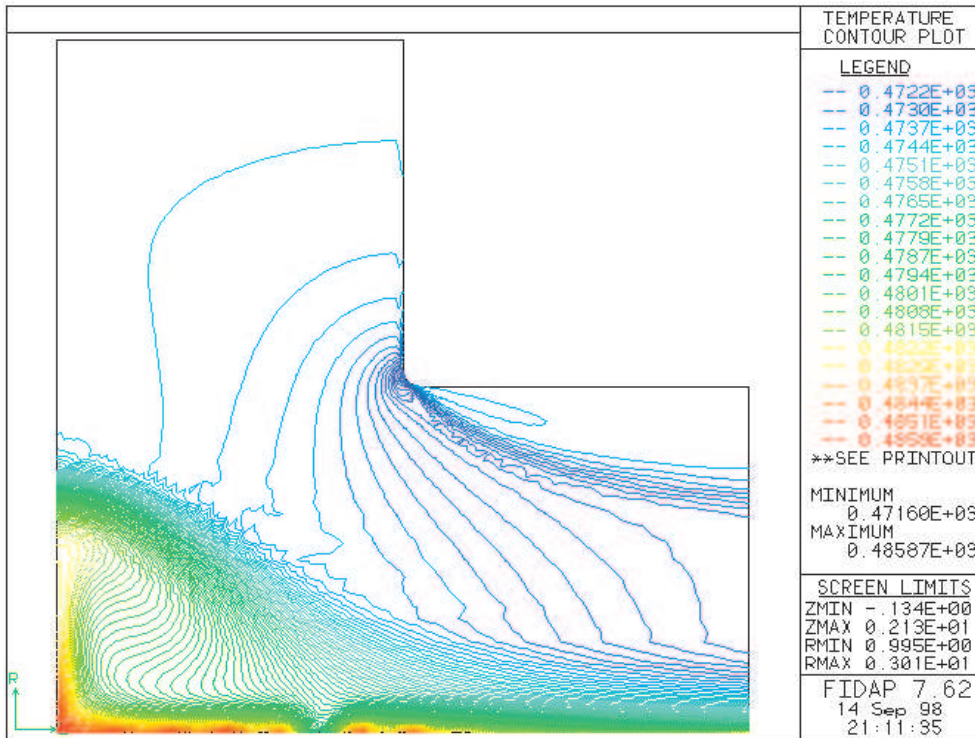


Figure 7. Temperature distribution

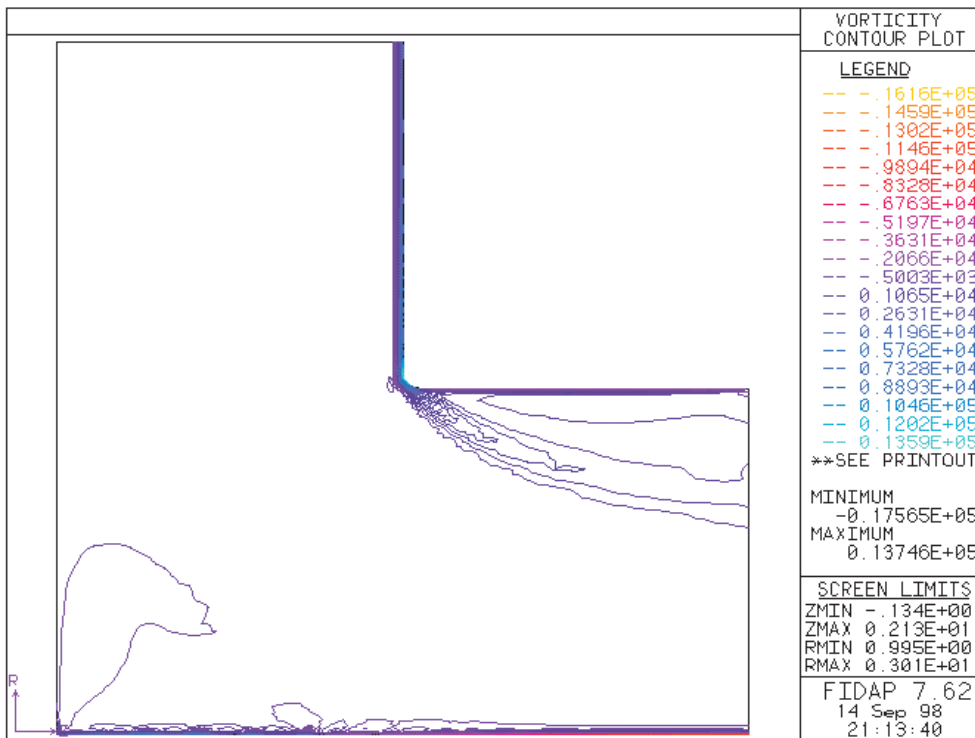


Figure 8. Vorticity distribution

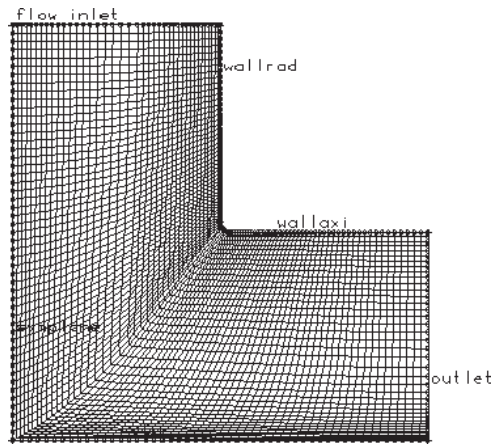


Figure 9. Mesh variant "A"

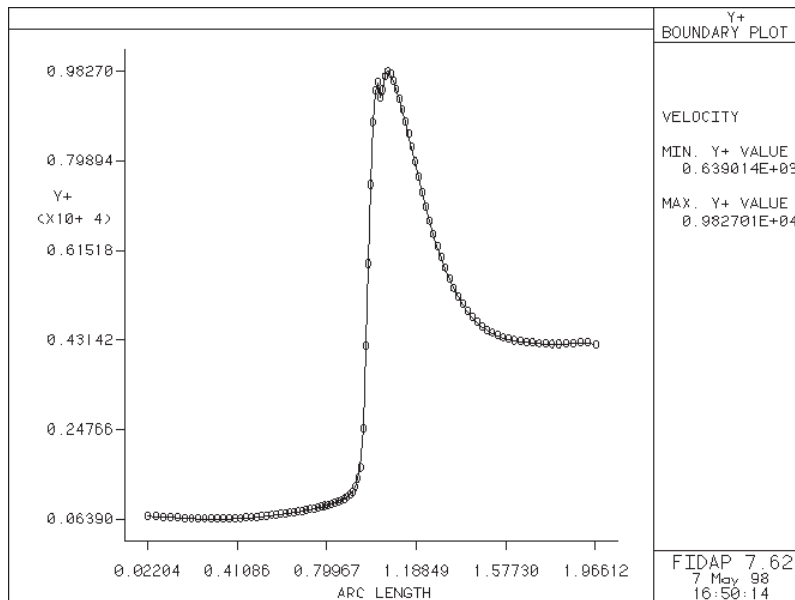


Figure 10. Corresponding y^+ distributions at fixed wall, variant "A"

to more closely resemble the uniform inflow case. It was observed that this considerable variation in velocity profiles had very little effect on the distribution of relevant outlet parameters (velocity and pressure), so it was deemed unnecessary to formulate other velocity distribution variants.

Varying turbulent intensity at inlet between the limiting cases of 0% and 10% also had only a minor effect on outlet parameters, but it did induce significant variation in other aspects of the flow, such as the extent of the standing vortices at the shaft and the distribution of dissipation over the investigated region. In general, the greater the turbulent intensity, the larger the vortices.

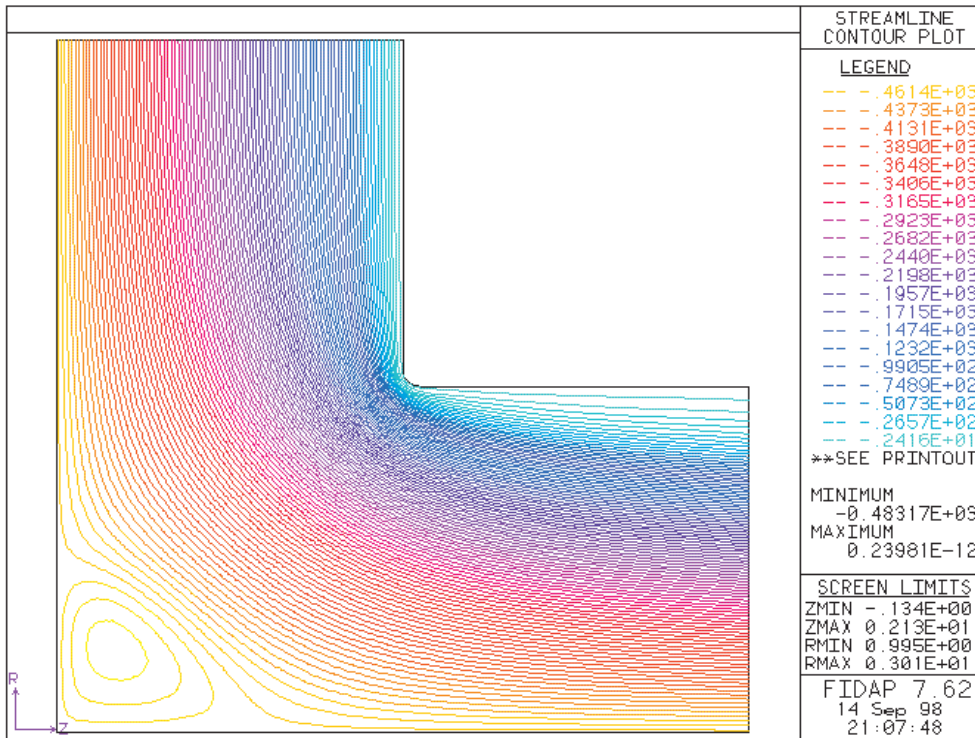


Figure 11. Streamline plot, variant "A"

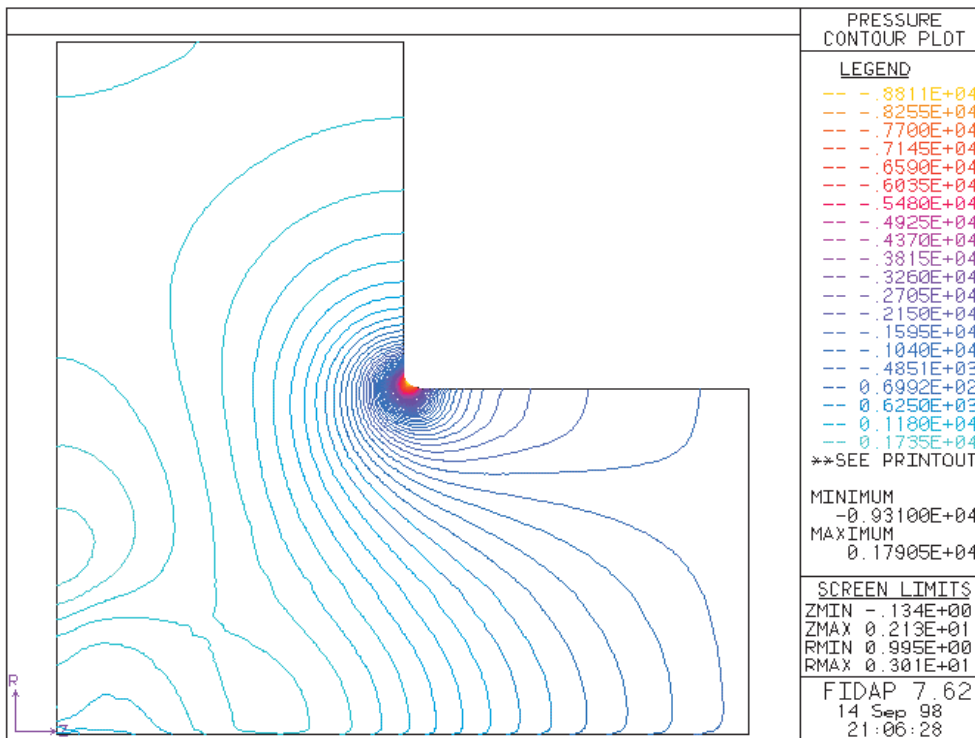


Figure 12. Pressure distribution, variant "A"

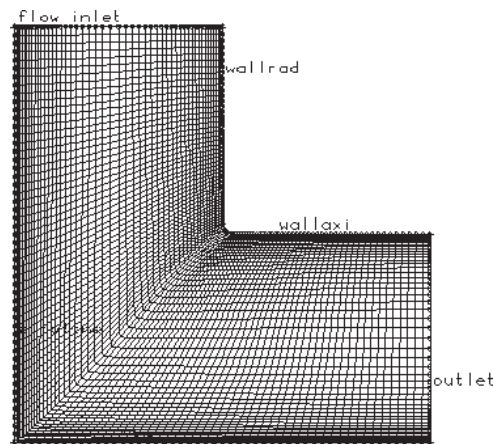


Figure 13. Mesh variant "B"

6. Conclusions

Variation of simulation results in response to changing boundary conditions at the inlet is generally to be expected; the degree of variation is the point of interest. On the other hand, the variation of results at constant boundary conditions, induced by changing the non-physical parameters such as turbulence model, numerical scheme, or mesh details constitutes a disturbing proof of the limited applicability of the individual computational procedures. The following set of examples illustrates two widely differing results obtained for the same boundary conditions (Figure 2) and the same turbulence model (RNG revised) for two differently spaced meshes and two different upwinding schemes.

Simulation run "A" was performed with a first-approximation meshing shown in Figure 9. The y^+ distribution along the fixed wall for this mesh is shown in Figure 10. (the visible peak corresponds to the rounded corner where the wall changes direction). The y^+ values obtained for this mesh, as may readily be noted, are too large (on the order of 6×10^3) in the entire region following the corner, which will likely result in incorrect modeling of near-wall flow in that region. The problem is not helped by the choice of an inadequate upwinding scheme (streamline upwinding, not the best when nonuniformity of flow is expected – a separation zone in this case). The resulting streamline plot is seen in Figure 11 – the streamlines follow the wall without separation, in spite of having passed through an adverse pressure gradient in the vicinity of the corner (Figure 12).

For simulation "B" the meshing was refined with an eye toward correcting the undesirable y^+ distribution on the horizontal portion of the wall, while retaining the same number of elements. The hybrid upwinding scheme was employed. The corrected meshing is shown in Figure 13.

The y^+ distribution at the fixed wall, for simulation "B", is shown in Figure 14. While there is still an unavoidable peak at the corner, the remaining values fall within acceptable limits.

Figure 15 shows the corresponding streamline plot for variant "B". There is a noticeable qualitative change in the pattern of the streamlines in the corrected region near the horizontal wall – a separation region is now apparent. This is also borne out by plotting axial velocity values at the outlet (Figure 16). The second plot shows a backflow near the fixed

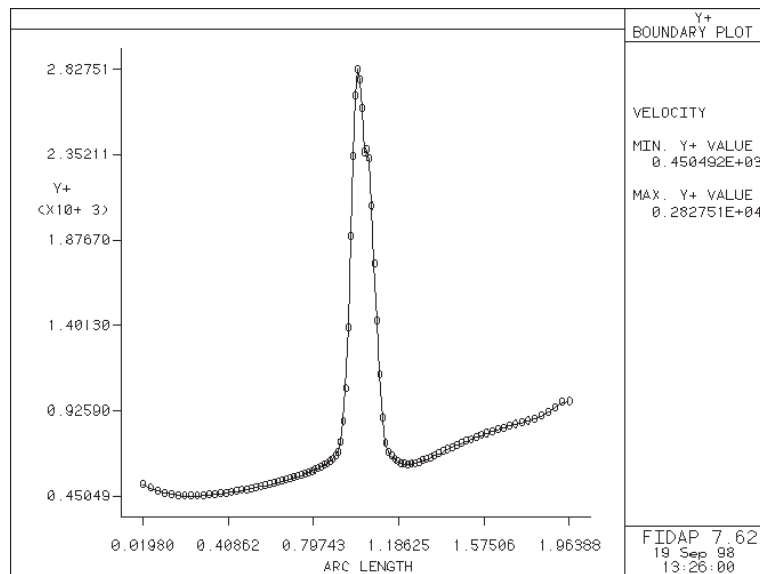


Figure 14. Corresponding y^+ distributions at fixed wall, variant "B"

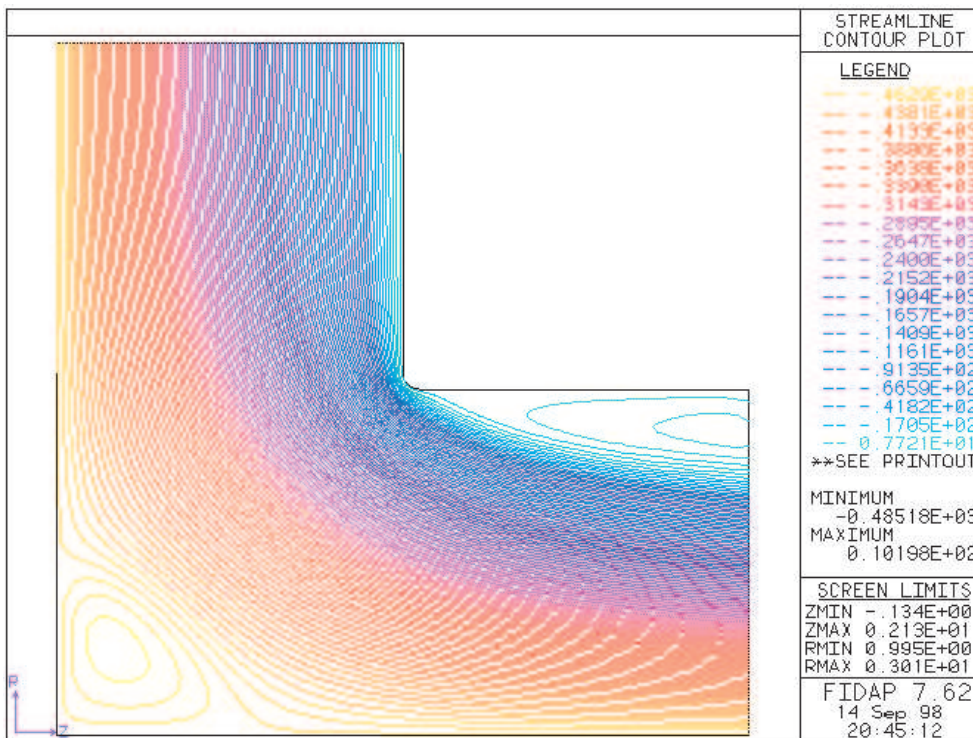


Figure 15. Streamline plot, variant "B"

wall. It should be stressed that physical flow parameters were identical for these two variants – a qualitative change in simulation results was brought about solely by manipulating non-physical parameters of the numerical model. The extent of this unwelcome variation can

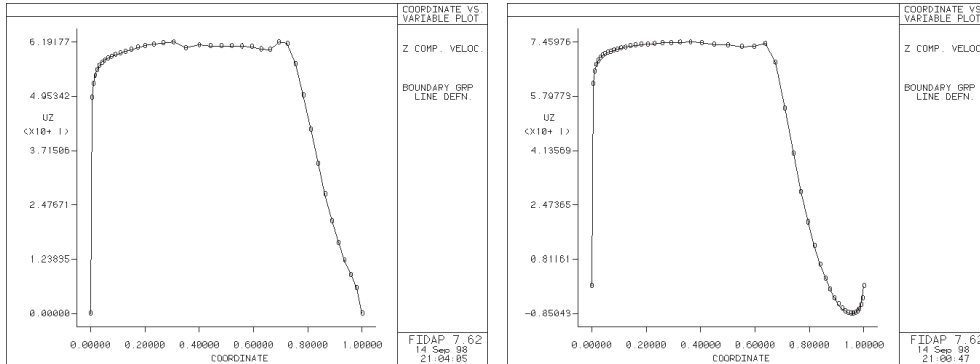


Figure 16. Axial velocity u_z profiles at outlet plane, variants “A” and “B”, respectively

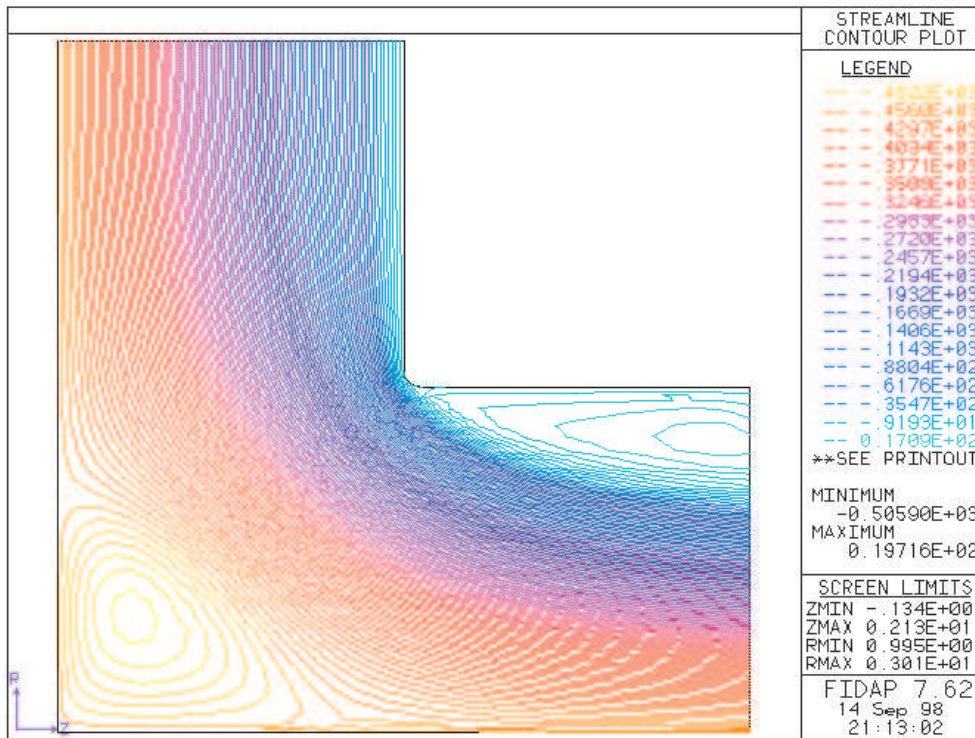


Figure 17. Streamline plot, variant “C”

best be gauged by introducing variant “C” for comparison. Variant “C” retains most of the parameters (including the meshing) of variant “B”; however, the flow is modeled as compressible.

As can be seen in Figure 17, the flow pattern closely resembles the incompressible variant, as does the axial velocity plot (Figure 18).

Clearly, the introduction of compressibility has less of an effect on the simulated flow than do minor details of meshing and refinements in the numerical scheme. Great care must therefore be exercised in near-wall meshing when setting up a flow simulation run, particularly when near-wall phenomena are likely to influence the gross flow pattern. By

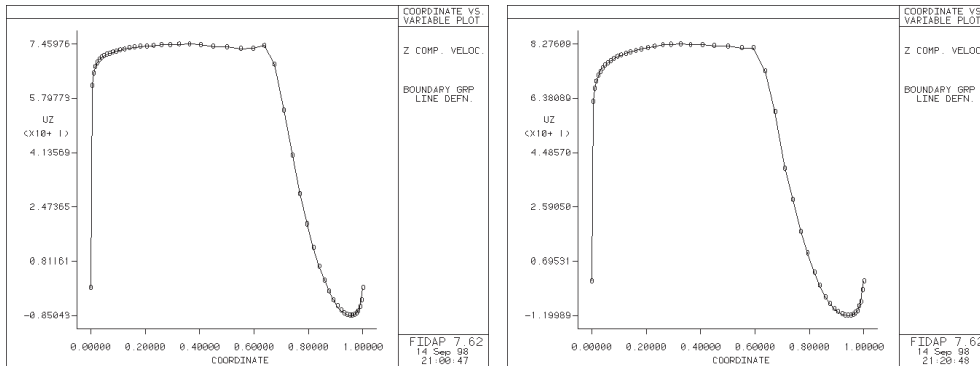


Figure 18. Axial velocity u_z profiles at outlet plane, variants “B” and “C”, respectively

analyzing such examples one may hope to better understand the strengths and limitations of the individual methods, and their appropriate applications.

Acknowledgements

The author wishes to convey thanks to the personnel at the TASK Academic Computing Center, without whose assistance and resources this work wouldn't have been possible.

References

- [1] Flaszynski P 1998 *Internal Report of the Turbomachinery and Fluid Mechanics Faculty*, Gdansk (in Polish)
- [2] Mekrouz K 1997 *Internal Report of the Turbomachinery and Fluid Mechanics Faculty*, Gdansk (in Polish)
- [3] Puzyrewski R 1998 *14 Lectures on the Theory of Turbomachinery Stages – 2D Model* Technical University of Gdansk, Gdansk (in Polish)